

Evidence for stepwise dissociation dynamics in acetone at 248 and 193 nm

Simon W. North, David A. Blank, J. Daniel Gezelter, Cheryl A. Longfellow,
and Yuan T. Lee

*Chemical Sciences Division, Lawrence Berkeley Laboratory, and Department of Chemistry,
University of California, Berkeley, California 94720*

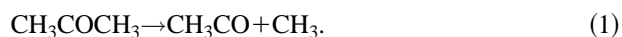
(Received 29 November 1994; accepted 8 December 1994)

The technique of molecular beam photofragment translational spectroscopy has been used to study the dissociation of acetone following $S_1 \leftarrow S_0$ (248 nm) and $S_2 \leftarrow S_0$ (193 nm) excitation. Excitation at 248 nm resulted in the production of CH_3 and CH_3CO with 14.2 ± 1.0 kcal/mole on average of the available energy appearing as translation of the photofragments. Comparison of the measured $\langle E_T \rangle$ with values reported at 266 nm suggest that the energy partitioning is dominated by the exit barrier caused by an avoided crossing on the potential energy surface. A substantial fraction ($30 \pm 4\%$) of the nascent acetyl radicals from the primary dissociation contain sufficient energy to undergo spontaneous secondary decomposition. From the onset of the truncation of the CH_3CO $P(E_T)$ a threshold of 17.8 ± 3.0 kcal/mole for the dissociation of the acetyl radical has been determined in agreement with recent results on the photodissociation of acetyl chloride. The translational energy release in the dissociation of CH_3CO closely matches the experimentally determined exit barrier. At 193 nm the only observed dissociation pathway was the formation of two methyl radicals and carbon monoxide. On average $\sim 38\%$ of the available energy is found in product translation suggesting that significant internal energy resides in the nascent CH_3 fragments consistent with the results of Hall *et al.* [J. Chem. Phys. **94**, 4182 (1991)]. We conclude that the dynamics and energy partitioning for dissociation at 193 nm is similar to that at 248 nm. © 1995 American Institute of Physics.

I. INTRODUCTION

Acetone, the simplest ketone, has been used as a model system for understanding the rich photochemistry of this entire class of carbonyl compounds. Photolysis proceeding via α -bond cleavage (Norrish type I) is the most studied of the photochemical processes. At sufficiently high excitation energies acetone represents a prototypical three-body dissociation process involving the cleavage of two identical chemical bonds. Of dynamical interest is the extent to which the two bond breaking steps are energetically and temporally coupled. The existence of spectroscopic methodology for probing the photofragments has resulted in the extraction of considerable information concerning the nascent energy distributions of the products. However, despite numerous recent studies on the photodissociation dynamics of acetone, the sequence of events leading to the three asymptotically separated fragments is still largely unresolved. The present experiments were pursued in order to further clarify the gas phase UV photodissociation dynamics of acetone.

The first absorption band in acetone centered at ~ 260 nm corresponds to an $\pi^* \leftarrow n(S_1 \leftarrow S_0)$ transition.¹ This involves promotion of a nonbonding electron on the oxygen to an antibonding orbital localized on the carbonyl moiety. Within this wavelength region acetone dissociates to yield methyl and acetyl radicals²



The initial excitation is to the A'' adiabatic potential energy surface which is bound along the C–C coordinate. Bond cleavage can occur by either internal conversion or intersystem crossing to the C_s ${}^3\sigma\sigma^*$ configuration via out-of-plane motion.^{3,4} Excited state dissociation then proceeds over a

small barrier caused by an avoided crossing on the T_1 surface. The barrier height has been measured by Zuckermann *et al.* who observed a pronounced decrease in the fluorescence emission at 305.8 nm. This corresponded to a barrier for dissociation of 93.4 kcal/mole above the ground state.⁵ Hancock and Wilson used photofragment translational spectroscopy (PTS) to examine the photodissociation dynamics at 266 nm and found that 13.9 kcal/mole on average of the available energy appeared as product translation.⁶ Waits *et al.* measured the translational energy of the vibrationless CH_3 radicals by 2+1 resonance enhanced multiphoton ionization (REMPI) ionization/time-of-flight mass spectrometry and obtained a similar $\langle E_T \rangle$ value.⁷ The large fraction of energy partitioned into translation of the photofragments was attributed by both groups to a barrier in the exit channel. The similarity between the observed translational energy release and the barrier height of 13.2 kcal/mole determined by Zuckermann *et al.* suggested that the dissociation proceeds on the T_1 surface. The spatial distribution of the photofragments in both studies^{6,7} was found to be isotropic, contrary to the work of Solomon *et al.* who observed anisotropy in the dissociation.⁸

The spontaneous decomposition of the acetyl radical is possible if its internal energy exceeds the barrier to dissociation



Kinetics studies of CH_3 addition to CO yielded a CH_3CO barrier to dissociation of 17.2 ± 0.5 kcal/mole.⁹ A number of other kinetic studies have obtained values ranging from 11.1 to 21.7 kcal/mole.¹⁰ In a more direct experiment Gandini and Hackett determined a barrier height of 20.3 kcal/mole from

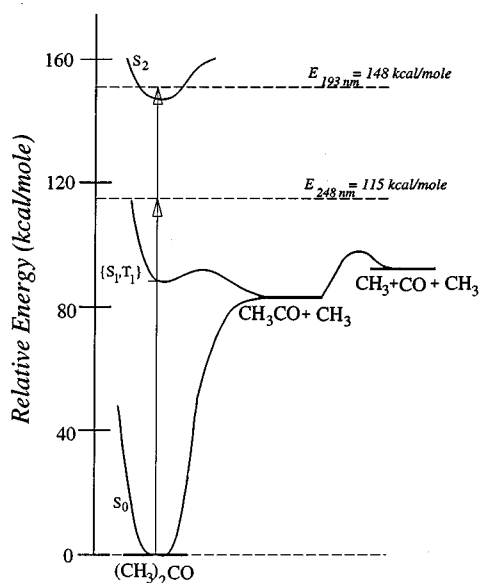


FIG. 1. Energy level diagram for acetone dissociation adapted from Ref. 19.

observing the CO ($A^1\Pi \rightarrow X^1\Sigma^+$) resonance fluorescence produced from acetone dissociation at 330–250 nm.¹¹ Deshmukh and Hess have detected $Cl(^2P_J)$ and CH_3 photoproducts by 2+1 REMPI arising from the 236 nm dissociation of acetyl chloride.¹² The quantum yield of CH_3 from CH_3CO decomposition was estimated at $\Phi_{CH_3} = 28\%$ although no barrier height was given. Recent PTS studies in our laboratory on acetyl chloride photodissociation at 248 nm showed that $\sim 35\%$ of the acetyl radical fragments underwent secondary decomposition.¹³ The barrier height to CH_3CO dissociation was determined to be 17 ± 1 kcal which is consistent with the result of Watkins and Word.

The second absorption band ($S_2 \leftarrow S_0$) in acetone results from an $3s \leftarrow n$ Rydberg excitation. The S_2 state is predissociative, coupling to the $\{S_1, T_1\}$ state via skeletal bends and CH_3 torsion.^{14,15} Figure 1 shows a schematic energy level diagram for the photodissociation of acetone. Pilling and co-workers have shown by end product analysis that dissociation into two methyl radicals and carbon monoxide



accounts for $>95\%$ of the photolysis products.¹⁶ This observation, in addition to the large absorption cross section at 193 nm demonstrated the potential of acetone as a clean source of methyl radicals for higher temperature kinetics studies. The first determination of the internal state distribution of a nascent photofragment was obtained from time resolved infrared emission of CO by Donaldson and Leone.¹⁷ The significant rotational excitation observed was attributed to a stepwise dissociation mechanism. Excitation in the $CH_3\nu_3$ vibration was also monitored and showed evidence for at least one methyl possessing substantial vibrational energy. Woodbridge *et al.* subsequently measured the CO distributions with higher resolution and concluded that the rotational temperature was slightly greater than observed by Donaldson (~ 3360 K).¹⁸ In a comprehensive study, Trentel-

man *et al.* measured the rovibrational and translational energy of all the photofragments.¹⁹ The CO distributions were obtained using rotationally resolved vacuum ultraviolet (VUV) laser-induced fluorescence ($A^1\Pi \leftarrow X^1\Sigma^+$) excitation spectroscopy and significant rotational excitation was observed. The translational energy of the CO fragment was also determined from the Doppler widths of several of the rovibronic transitions. Linewidths of $0.5\text{--}0.6\text{ cm}^{-1}$ were attributed to a center-of-mass velocity of 1600 m/s and a kinetic energy of 8.6 ± 1.0 kcal/mole. The methyl fragments were probed via 2+1 REMPI through the $3p^2A_2'' \leftarrow 2p^2A_2'$ transition and observed to be vibrationally cold (76% in $\nu=0$) with most of the vibrational energy in the ν_2 mode. Using the pulsed field extraction time-of-flight technique, Trentelman *et al.* measured the translational energy of the $CH_30_0^0$ band to be 10.5 ± 2 kcal/mole. The translational energy distributions for both methyl radicals were found to be indistinguishable. The low internal energy content of the methyl fragments was interpreted by Trentelman as evidence for a dissociation which occurred prior to randomization of the available energy.¹⁹ Recent diode laser absorption/gain experiments on the 193 nm photolysis of acetone- d_6 by Hall *et al.* suggest, however, that the vibrational energy excitation of the nascent methyl radicals is significantly higher.²⁰ A *stepwise dissociation* involving almost complete randomization is consistent with the observed 6% population of CD_3 photofragments formed in the vibrationless state.

By measuring the translational energy of all the photofragments averaged over all product quantum states we hope to obtain a more complete picture of the dissociation dynamics. Photodissociation at 248 nm represents an important extension of earlier work performed at 266 nm. The variation in the partitioning of available energy into product translation as a function of excitation wavelength within the same absorption band can reveal much about the topology of the potential energy surface. In addition, photodissociation at 248 nm presents the opportunity to extract additional evidence concerning the barrier height to CH_3CO decomposition as well as its unimolecular dissociation dynamics. In light of the recent disparate dissociation mechanisms proposed by Hall and Trentelman, the photodissociation of acetone at 193 nm clearly warrants further investigation. The translational energy distribution of the CH_3 photofragments following 193 nm ($S_2 \leftarrow S_0$) excitation have previously been measured for only the vibrationless methyl products. It is our belief that a remeasurement of this particular degree of freedom is crucial to determining the true partitioning of the available energy.

II. EXPERIMENT

These measurements were carried out on a molecular beam apparatus with a fixed source and a rotatable detector that has been adapted to perform photofragment translational spectroscopy experiments.^{21,22} For the majority of the experimental data acetone seeded in helium was expanded using a pulsed valve²³ (1.0 mm nozzle) with a Physik-Instrumente piezocrystal. The conditions of the molecular beam varied from 5%–20% acetone at stagnation pressures ranging be-

tween 150–680 Torr. An extension on the pulsed valve nozzle heated to 200 °C significantly reduced formation of clusters in the beam. A time-of-flight method was used with a spinning slotted wheel to measure the velocity and velocity spread of the molecular beam. An appropriate time delay between the wheel and the pulsed valve ensured accurate sampling of the region of the pulse that was irradiated.

The resulting collimated pulsed beam was crossed at 90° with the output of a Lambda Physik EMG 202 MSC excimer laser operating at the ArF (193.3 nm) and KrF (248.5 nm) transitions. The laser fluence at both wavelengths was typically 40–160 mJ/cm². The neutral photofragments recoiled 20.8 cm where they were ionized by electron bombardment, mass selected using a quadrupole mass spectrometer, and counted with a Daly ion detector. A computer interfaced multichannel scaler, triggered from the laser pulse, was used to collect and store the data. Polarization of the laser was achieved with ten quartz plates at Brewster's angle with respect to the direction of laser propagation. The resulting >95% polarized light could then be rotated by adjusting the orientation of the polarizer.

The data was fit using an iterative forward convolution technique that has been previously described.^{24,25} Briefly, a center-of-mass translational energy distribution is chosen, convoluted with the instrument response functions, and transformed into laboratory time-of-flight (TOF) spectra. The calculated TOF is then compared to the experimental TOF and the translational energy distribution is iteratively adjusted until a satisfactory fit is obtained.

III. RESULTS AND ANALYSIS

A. Excitation at 248 nm

Product time-of-flight data was collected for $m/e=15$ (CH_3^+), $m/e=28$ (CO^+), and $m/e=43$ (CH_3CO^+) at detector angles ranging from 15° to 55° from the molecular beam. Subtraction of the laser-off spectra from the laser-on spectra was performed on all time-of-flight spectra. The $m/e=15$ TOF spectra shown in Fig. 2 consists of three components: methyl radicals and acetyl radicals from reaction (1) and secondary methyl radicals from reaction (2).

The fast peak at $\sim 60 \mu\text{s}$ in Fig. 2 corresponds to methyl radicals from reaction (1). The energy available to be partitioned between the degrees of freedom of the primary photofragments is given by the following expression

$$E_{\text{avail}} = E_{h\nu} - D_0(\text{CH}_3\text{CO}-\text{CH}_3) + E_{\text{int}}, \quad (4)$$

where $E_{h\nu}$ is the photon energy (115 kcal/mole), $D_0(\text{CH}_3\text{CO}-\text{CH}_3)$ is the bond dissociation energy of 83.7 kcal/mole (Ref. 26) and E_{int} is the internal energy of the parent molecule. The vibrational energy content of acetone at room temperature is estimated to be ~ 1.5 kcal/mole based on the known vibrational frequencies.²⁷ Most of this excitation should involve the low frequency modes, skeletal bends and methyl torsions, which are expected to undergo partial or complete relaxation in the supersonic expansion. Assuming that the internal energy of the parent is negligible, the available energy is 31.3 kcal/mole following C–C bond cleavage. The total center-of-mass translational energy distribution for

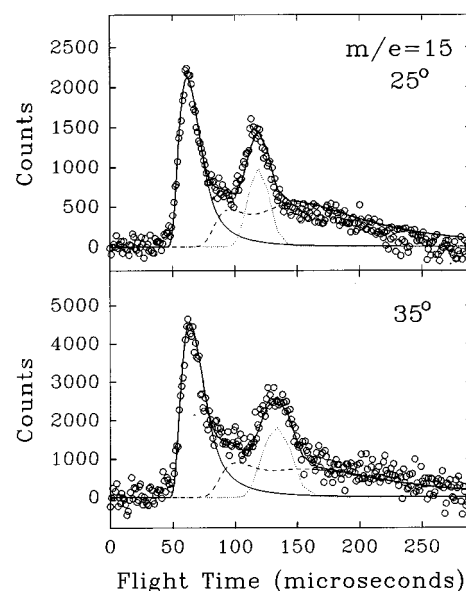


FIG. 2. TOF spectra at 248 nm of $m/e=15$ (CH_3^+) at laboratory angles 25° and 35°. Circles represent data points. Contributions are shown for CH_3 (solid line) and CH_3CO (dashed line) from reaction (1) and CH_3 originating from reaction (2) (dotted line).

reaction (1) which was derived from fitting the fast component in Fig. 2 is shown by the solid line in Fig. 3. The $P(E_T)$ has an average value of 14.2 ± 1.0 kcal/mole and a full width at half maximum (FWHM) of ~ 12 kcal/mole corresponding to an average of 45% of the available energy appearing as product translational energy.

At longer times ($\sim 130 \mu\text{s}$) in Fig. 2 is a peak from dissociatively ionized CH_3CO . Since the acetyl radical is the momentum matched fragment of the primary methyl it should share the same $P(E_T)$. However, the slow component is noticeably absent from the TOF profile. This is more evi-

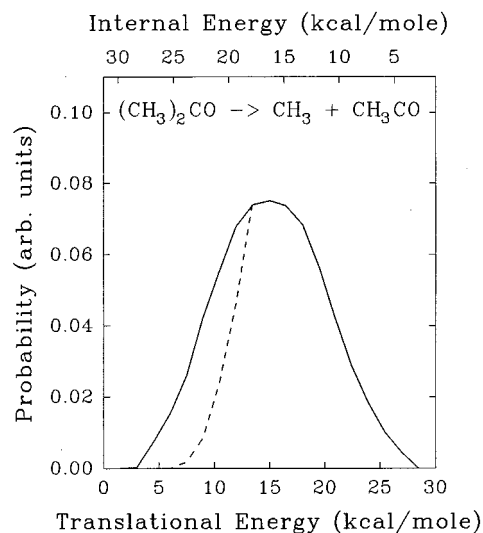


FIG. 3. Center-of-mass translational energy distribution, $P(E_T)$ for reaction (1) used to fit the data in Figs. 2 and 4. The solid line is derived from fitting the methyl radical from reaction (1) and the dotted line is derived from fitting the $m/e=43$ spectra.

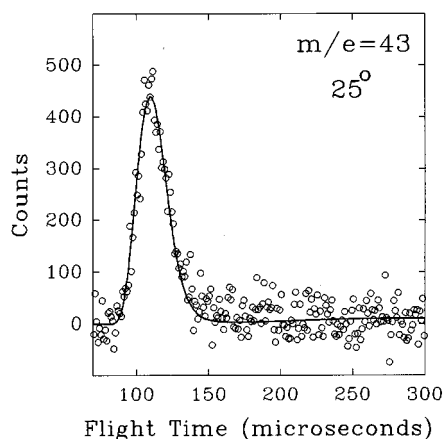


FIG. 4. TOF spectrum at 248 nm of $m/e=43$ (CH_3CO^+) at a laboratory angle of 25° . Circles represent data points and the line is the forward convolution fit using the $P(E_T)$ in Fig. 3 truncated as shown by the dotted line.

dent in the $m/e=43$ (CH_3CO^+) TOF spectra shown in Fig. 4. By conservation of energy, the smaller the translational energy of the photofragments the greater their internal excitation. When the internal energy exceeds the barrier to dissociation of CH_3CO these radicals fail to persist long enough to reach the detector. This resulting truncation of the low energy CH_3CO radicals is illustrated in the center-of-mass velocity distributions of Fig. 5. A dotted line that starts to deviate from the CH_3 $P(E_T)$ in Fig. 3 at ~ 12 kcal/mole marks the truncation of the low energy side of the CH_3CO $P(E_T)$. The $m/e=43$ spectrum at 25° was used to fit the slow portion of the CH_3CO $P(E_T)$ and yields a reasonable fit to the slow component in the $m/e=15$ TOF spectra (Fig. 4). Based on the relative integrated area of the truncated region to the entire primary $P(E_T)$ an estimate of the fraction of acetyl radicals that undergo secondary dissociation can be obtained. This gives a value of $30\% \pm 4\%$ which is in good agreement with the CO quantum yield of 0.35 determined at 250 nm by Gandini and Hackett.¹¹ The uncertainty reflects our measure of confidence in fitting the slow side of the $m/e=43$ peak in the TOF spectra.

The $m/e=43$ TOF spectra for vertical and horizontal linear polarization of the photolysis laser showed no difference in intensity. The acetyl radical fragment was monitored because the TOF flight spectra have only a single component

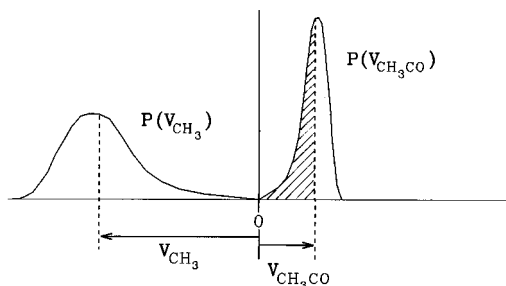


FIG. 5. Center-of-mass velocity distributions for CH_3 (left) and CH_3CO (right) from reaction (1). The shaded region indicates CH_3CO radicals that are unstable with respect to secondary dissociation.

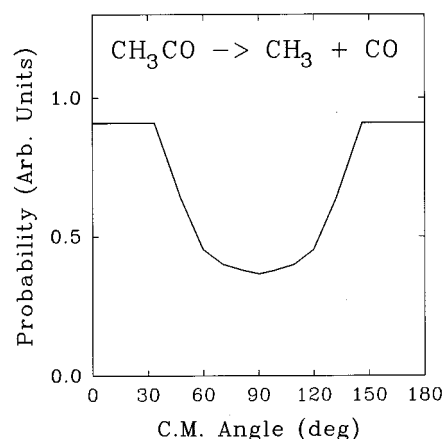


FIG. 6. Center-of-mass angular distribution, $T(\theta)$, used to fit the secondary fragments from reaction (2). 0° corresponds to the direction of the acetyl radical recoil.

and superior signal-to-noise compared to $m/e=15$. The absence of any correlation between the fragments recoil and the angle of laser polarization is consistent with the findings of Refs. 6 and 7 but contrary to the anisotropy reported in Ref. 8. An anisotropy parameter²⁸ of $\beta=0$ was used to fit the entire set of experimental data.

The last component of the $m/e=15$ TOF in Fig. 2 is a broad underlying feature due to methyls from the secondary decomposition of acetyl radicals [reaction (2)]. Since this feature arises from acetyl radicals that are absent from the total $P(E_T)$ for reaction (1), the primary distribution of CH_3CO translational energies was obtained by subtracting the CH_3CO $P(E_T)$ from the *true* primary $P(E_T)$ used to fit the CH_3 radicals from the initial bond cleavage step. In order to fit the apparent bimodal shape in the TOF, a forward-backward symmetric secondary angular distribution, $T(\theta)$, was used, consistent with the fated acetyl radicals persisting for longer than their rotational period.²⁹ The secondary angular distribution is shown in Fig. 6. The fits to the secondary components of the TOF spectra were reasonably sensitive to both the secondary $P(E_T)$ and $T(\theta)$. Provided that the forward-backward symmetry, peaking along the poles, of $T(\theta)$ was maintained and the secondary $P(E_T)$ was peaked ~ 5 – 7 kcal/mole away from zero, reasonable fits to the data could be achieved. We, therefore, adopted a simple model in which the primary and secondary $P(E_T)$'s were decoupled but constrained to conserve the available energy. This resulted in appropriate truncation of the secondary $P(E_T)$ when required. The best fit was obtained with a broad Gaussian secondary $P(E_T)$ with a most probable value that closely matched the experimental exit barrier height (~ 6 kcal/mole).^{9,13} Figure 7 shows the $m/e=28$ (CO^+) TOF spectrum at a laboratory angle of 35° . The spectrum contains contributions from primary acetyl fragments and CO from reaction (2). The secondary $T(\theta)$ and $P(E_T)$, derived from acetone dissociation, were also used with only slight modification to fit successfully the CH_3 TOF spectra arising from the secondary CH_3CO decomposition in the photodissociation of CH_3COCl (Ref. 13) and CH_3COBr (Ref. 30) at 248

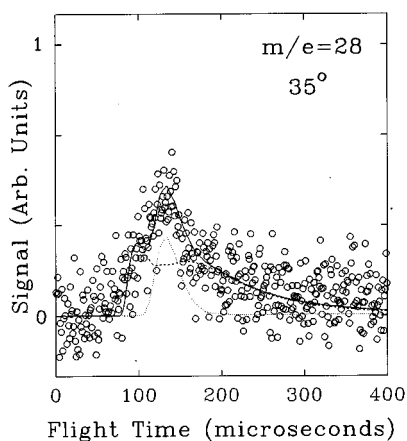


FIG. 7. TOF spectrum of $m/e=28$ (CO^+) at 248 nm. The open circles are the data. The lines are the contributions from primary acetyl fragments (dashed line) and CO fragments from secondary dissociation.

nm as shown in Fig. 8. The insets of Fig. 8 show the primary translational energy distributions derived from fitting the respective halogen atoms.

The intensity of all detected fragments from acetone photodissociation varied linearly with laser power indicating that the observed processes involve a single photon.

B. Excitation at 193 nm

Time-of-flight spectra for $m/e=15$ and $m/e=28$ were collected at detector angles ranging from 15° to 55° . Signal was not observed at $m/e=43$, the parent mass of the acetyl radical. Although CH_3CO could dissociatively ionize to

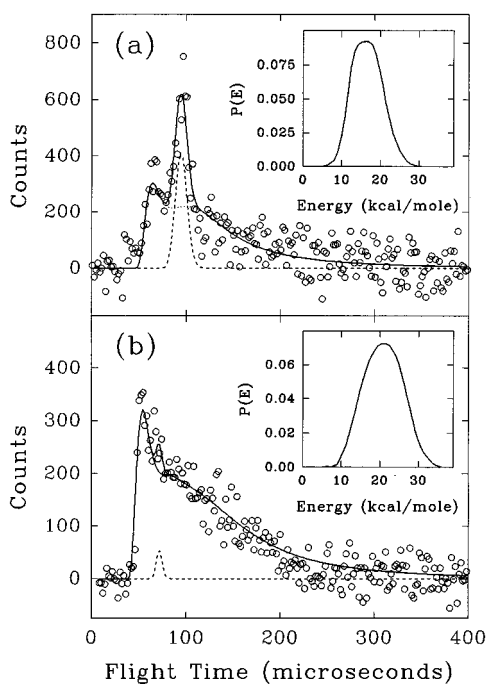


FIG. 8. TOF spectra of $m/e=15$ (CH_3^+) at a laboratory angle of 20° from the 248 nm photodissociation of (a) CH_3COCl and (b) CH_3COBr . The open circles are the data and the contributions are identical to those in Fig. 7 (see text for details).

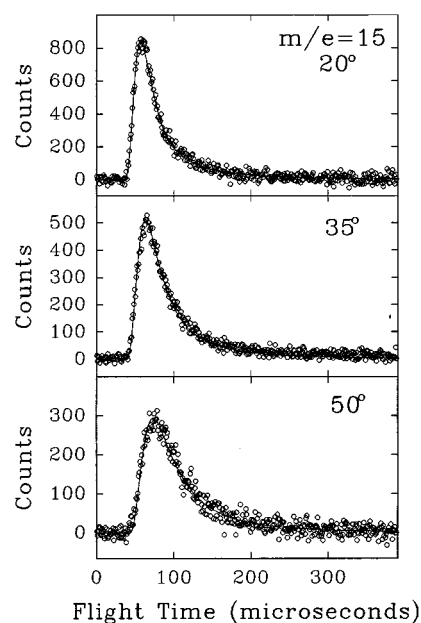
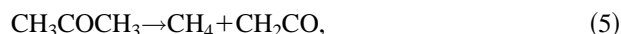


FIG. 9. TOF spectra at 193 nm of $m/e=15$ (CH_3^+) at laboratory angles 20° , 35° , and 50° . Circles represent the data and the line is the forward convolution fit using the $P(E_T)$ in Fig. 10.

lower masses, there was no evidence for acetyl at its daughter masses. TOF spectra were also measured at several other masses that would correspond to the products from the following proposed minor channels in the 193 nm photolysis of acetone:¹⁶



No photodissociation signal was detected at $m/e=16$ (CH_4^+) or $m/e=42$ (CH_2CO^+) that would arise from reaction (5). In order to ascertain the importance of reaction (6) the experimental apparatus was modified to facilitate the detection of hydrogen atoms.³¹ The only single photon laser dependent signal observed at $m/e=1$ was due to methyl radicals from reaction (3) that had dissociatively ionized.³² Although reactions (5) and (6) may still be occurring at levels below the limit of our detection they are minor channels.

Time-of-flight data for $m/e=15$ at laboratory angles of 20° , 35° , and 50° are shown in Fig. 9. The observation of only a single peak in the TOF spectra is consistent with the indistinguishability of the velocity distributions reported by Trentelman.¹⁹ If the single peak is the result of methyls originating from a synchronous three-body dissociation then, since the methyl radicals are identical, the treatment of the data is straightforward. A method for the analysis of a synchronous dissociation was recently developed for the study of *s*-tetrazine and a thorough description of the method is presented therein.³³ Briefly, the experimental data is analyzed by the same forward convolution technique used to fit two-body dissociations but with several important differences. First, an energy independent set of most probable angles between the asymptotic velocity vectors is chosen. Gaussian functions describe the spread about these angles and a total

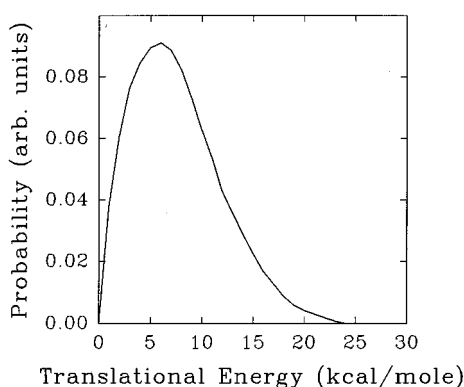


FIG. 10. Center-of-mass translational energy distribution derived from fitting the $m/e=15$ TOF spectra at 193 nm.

translational energy distribution is assumed. All three are then iteratively adjusted until a satisfactory fit to the data is obtained. The present data could not be fit in this manner by constraining the dissociation to be symmetric about the two C–C–O angles.³⁴ This suggests that a *nonsynchronous dissociation* with overlapping CH_3 distributions is more probable than a synchronous one. This is consistent with the high degree of CO rotation observed previously.^{17–19} Since the dissociation is nonsynchronous, involving two impulses separated by a finite time interval, the inability to resolve the two methyl radicals makes a unique determination of the translational energy distributions from each step impossible.

The least biased approach to fitting the methyl TOF spectra involves obtaining the independent fragment $P(E_T)$ for the methyl radical in the acetone center of mass. Figure 10 shows the distribution which has an average value of 7.7 ± 1.0 kcal/mole and a FWHM of ~ 15 kcal/mole. The CO fragment ($m/e=28$) TOF spectra at laboratory angles 35° and 50° are shown in Fig. 11. In a similar fashion the CO

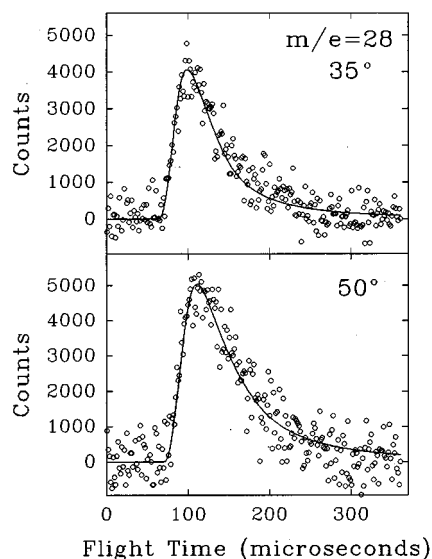


FIG. 11. TOF spectra at 193 nm of $m/e=28$ (CO^+) at laboratory angles 35° and 50° . Circles represent data points and the line is the best fit to the data.

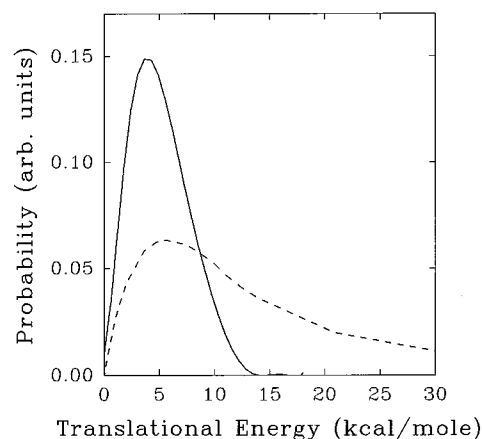


FIG. 12. Center-of-mass translational energy distribution derived from fitting the $m/e=28$ TOF spectra (solid line). The dashed line shows a Boltzmann distribution at 3000 K.

$P(E_T)$ can be derived (Fig. 12) and has an average value of 4.8 ± 0.5 kcal/mole.

Polarization measurements were performed at both $m/e=15$ and $m/e=28$. The $m/e=15$ spectra exhibited no variation in either intensity or shape with the change of laser polarization. Since the single peak in the TOF spectra is a composite of methyl fragments from both the first and second bond cleavages, the ability to measure a small degree of anisotropy in the initial dissociation step is dubious. However, the lack of any apparent polarization dependence suggests that if the dissociation is not completely isotropic the anisotropy parameter is negligibly small.

IV. DISCUSSION

A. Excitation at 248 nm

Primary dissociation: The large fraction of available energy that is found in product translation for reaction (1) is not indicative of typical simple bond rupture via a loose transition state.³⁵ In that case, the translational energy would reflect the statistical partitioning of available energy into the reaction coordinate and produce a distribution peaked close to zero. The preponderance of energy that appears as fragment recoil could have several origins. Incomplete randomization of the available energy could leave a greater than statistical fraction in the reaction coordinate. This, however, seems difficult to reconcile given the available energy and a $^1(n, \pi^*)$ lifetime at 260 nm of 1 ns measured by Breuer and Lee.³⁶ A limiting, impulsive model for predicting the disposal of available energy between the translation and internal motion of the photofragments has been presented for triatomics by Busch and Wilson.³⁷ A generalization of the model to treat polyatomics has been developed by Tuck.³⁸ The *impulsive* approximation assumes that all of the available energy appears in the dissociative coordinate as repulsion between the two atoms linked by the dissociating bond. The remaining atoms are then considered as spectators and the redistribution of the initially localized energy proceeds in accordance with classical kinematics. The impulsive model

predicts that 54% of the available energy should appear as fragment translation. Interestingly, the $\langle E_T \rangle$ reported here (14.2 ± 1.0 kcal/mole) is very similar to the $\langle E_T \rangle$ values determined at 266 nm (13.9 kcal/mole) despite a difference of ~ 8 kcal/mole in the available energy. Since the energy partitioning in the impulsive model is based solely on mass factors, the fraction of the available energy in translation should be invariant with respect to the excitation energy. The agreement between the impulsive model and the experimental translational energy release at 266 nm is therefore fortuitous. The insensitivity of the photofragment translation to the excitation energy suggests that the dissociation dynamics are mediated by the substantial exit barrier on the potential energy surface. The origin of this barrier is an avoided crossing on the T_1 surface which is reached via intersystem crossing (ISC) from the excited S_1 state. If intramolecular vibrational redistribution (IVR) occurs prior to dissociation, as implied by the excited state lifetime of ~ 1 ns, then the translational energy release will be dominated by the repulsive forces acting beyond the transition state rather than the magnitude of the available energy. Dissociation will occur when sufficient energy, which is statistically redistributed among the vibrational modes of the parent, flows into the reaction coordinate to overcome the barrier on the potential energy surface. Photofragment translation, therefore, increases with available energy in proportion to the probability of finding excess energy in the reaction coordinate. This dependence is small, affecting mostly the width of the energy distribution, in comparison to the large translational energy release originating from the exit barrier.

There are many reasons why the photodissociation of a polyatomic molecule would lead to an isotropic spatial distribution of the fragments. Several of these have been discussed in regards to $^1(n, \pi^*)$ excited acetone.⁶ If the dissociation is less than prompt, the correlation between the direction on the electric dipole moment (μ) and the relative velocity vector (ν) of the photofragments will be diminished by parent rotation. Once the lifetime of the excited acetone exceeds several rotational periods then the angular distribution will approach isotropic. Given the ~ 1 ns lifetime of the S_1 state, rotation prior to dissociation appears to be a plausible explanation for the lack of observed spatial anisotropy.

Secondary dissociation: Photofragment translational spectroscopy has been successful in determining the energetics of radical decomposition by comparing the time-of-flight spectra for a radical photofragment and its momentum matched partner. This has been demonstrated by Minton *et al.* in determining the exothermicity of C_2H_4Cl dissociation³⁹ and more recently has been applied to the case of the acetyl radical.¹³ Although the acetyl radical can undergo secondary dissociation, the primary methyl radical cannot. The truncation of the CH_3CO $P(E_T)$ represents the maximum product internal energy at which the CH_3CO is stable. If $E_{T(\min)}$ denotes the value corresponding to the onset of truncation then the barrier to CH_3CO dissociation can be calculated from the following expression:

$$\begin{aligned} E_{\text{barr}}(CH_3-CO) &= E_{h\nu} - D_0(CH_3CO-CH_3) - E_{T(\min)} \\ &= E_{\text{avail}} - E_{T(\min)} \\ &= 31.3 - 13.5, \\ E_{\text{barr}}(CH_3-CO) &= 17.8 \pm 3.0 \text{ kcal/mole.} \end{aligned} \quad (7)$$

It is assumed that acetone, following supersonic expansion, possesses negligible internal energy. Rice–Ramsperger–Kassel–Marcus (RRKM) calculations indicate that acetyl radicals with 0.1 kcal/mole in excess of the barrier to dissociation have a lifetime of $\sim 5 \times 10^{-10}$ s, far shorter than the $\sim 1 \times 10^{-5}$ s flight time to the detector. Consequently the uncertainty introduced by the detection of acetyl radicals at energies just above the CH_3CO threshold to dissociation is minor. There are several factors that contribute to the less-than-abrupt truncation of the CH_3CO $P(E_T)$. The first is that a fraction of the product internal excitation can be partitioned into the methyl radical fragment. A detailed determination of the nascent rovibrational distributions of the methyl radical products has not been done at 248 nm although experiments at 266 nm have shown minor CH_3 excitation in the out-of-plane mode.⁷ As a consequence, some internal energy above the threshold for CH_3CO stability can be accommodated by the CH_3 partner fragment. As some of the available energy is partitioned into the internal degrees of freedom in the methyl fragment, the truncation will become more gradual. However, as long as a non-negligible quantity of internally cold CH_3 is produced, the onset of the truncation will still reflect the barrier height to CH_3CO dissociation. Another effect that may result in an overestimation of $E_{\text{barr}}(CH_3-CO)$ is rotational metastability of the CH_3CO fragment. From consideration of the nonplanar acetone transition state geometry, the acetyl fragment should contain ~ 1 kcal/mole of rotational energy. The angular momentum will be projected predominantly along the C–C bond and therefore most of this energy will be unavailable to couple into the reaction coordinate. A severe example of this effect was observed in the dissociation of bromoethanol by Hints *et al.* which, following initial C–Br bond cleavage, produces a highly rotationally excited C_2H_4OH radical that could be detected despite containing internal energy in excess of its barrier to dissociation.^{29d} The barrier height of 17.8 ± 3.0 kcal/mole should, therefore, be viewed as an upper limit. Since none of these factors are present in the photodissociation of acetyl chloride, the 17 ± 1 kcal/mole value obtained in that experiment is more reliable.

The secondary $T(\theta)$ and $P(E_T)$ derived from fitting the $m/e=15$ and $m/e=28$ TOF spectra provide a detailed measure of the dissociation dynamics of the acetyl radical. In order for the secondary angular distribution of a long-lived complex to be justified the lifetime of the acetyl radicals that dissociate would need to be longer than their respective rotational periods. Treating the CH_3CO as rigid, its rotational excitation can be calculated based on the exit impact parameter derived from the dissociative geometry and the most probable recoil velocity of the primary fragments. A nonplanar dissociation, consistent with the geometry of the transition state,³ predicts a rotational period of < 1 ps. RRKM calculations were performed using the vibrational frequencies of the radical and activated complex given by Watkins

and Word.⁹ Given an average internal energy of 24 kcal/mole for those CH₃CO radicals that decompose and our experimentally determined barrier height of 17.8 kcal/mole, a lifetime of ~10 ps is predicted which is longer than the rotational period. The present observations are also consistent with long-lived CH₃CO seen in the photodissociation of acetyl iodide^{29b} where the rotational excitation of the acetyl radical should be considerably less since the dissociation geometry is planar. In addition, the nascent CH₃CO radicals from acetyl iodide photodissociation contain ~45 kcal/mole of internal energy and should, therefore, possess much shorter lifetimes.

The remarkable similarity between the average translational energy of the secondary step and the exit barrier to CH₃CO decomposition suggests that the dissociation dynamics of the radical are analogous to the initial C–C bond cleavage in acetone, i.e., the energy partitioned into translation is determined by the repulsive forces acting in the exit channel. Further evidence to support this claim rests in the nearly identical secondary $P(E_T)$ required to fit the CH₃ and CO fragments from CH₃CO decomposition in the photodissociation of acetyl chloride and acetyl bromide despite the significantly different vibrational energy content of the nascent acetyl radical photofragments.

B. Excitation at 193 nm

Energy partitioning: Complementary product state distributions of the photofragments arising from acetone photodissociation at 193 nm have provided valuable insight into the dynamics of the bond breaking process. Donaldson,¹⁷ and later Woodbridge,¹⁸ both concluded that a nonsynchronous dissociation was necessary to account for the angular momentum reflected in the highly excited CO rotational distributions. Measurement of the ν_3 emission from the nascent CH₃ fragments by Donaldson suggested that at least one of the methyl radicals possessed significant vibrational energy. Based on these two observations Donaldson proposed that the dissociation was a two-step process although the time scale between C–C bond cleavages could not be unambiguously determined. A stepwise dissociation mechanism was supported by the work of Baba *et al.* who saw evidence for long-lived CH₃CO in the intensity dependent signal of CH₃CO⁺.⁴⁰ Trentelman, however, found that the CH₃ fragments probed using 2+1 REMPI contained little internal excitation and substantial translation energy.¹⁹ Both statistical and impulsive model predictions were compared to the experimental results in an effort to discern the dissociation dynamics. Statistical models were found to overestimate gravely the partitioning of the available energy into CH₃ vibration while underestimating the translational energy of all the fragments. The severe failure of the statistical models suggested that no randomization of the available energy occurs prior to *either* the first or second C–C bond cleavage. A modified impulsive model^{37,38} was utilized in which the energy available to all three asymptotic fragments was partitioned equivalently between the two C–C bonds and the dissociation then treated as two independent impulses in two center-of-mass reference frames that conserved momentum. It was assumed that following the first bond cleavage all the

TABLE I. Average fragment energies (kcal/mole) for acetone photodissociation at 193 nm.

	Ref. 19	Impulsive model ^a	This work	BIM ^b
$E_T(\text{CH}_3)$	10.5±1.9	10.5	10.5±0.5	10.7
$E_{\text{int}}(\text{CH}_3)$	2.6	2.6	...	17.2
$E_T(\text{CO})^c$	6.6±1.2	6.7	2.3±0.5	2.1
$E_{\text{int}}(\text{CO})$	9.1	10.3	...	5.7
$E_T(\text{CH}_3)^c$	12.1±1.9	14.3	4.3±0.5	4.0
$E_{\text{int}}(\text{CH}_3)$	2.6	3.6	...	9.4

^aThe method is outlined in Ref. 19.

^bThe details of the calculation are presented in the Appendix.

^cTranslational energies for these fragments are given in the secondary center of mass.

vibrational energy of the acetyl fragment was coupled into the second C–C bond cleavage. Favorable agreement between the model and the experimental results supported the conclusion that the dissociation involved almost no randomization of the available energy between either bond breaking step. The measured average energies in the various degrees of freedom of the fragments as well as the predictions of the impulsive model are shown in Table I.

Although the impulsive model was successful in matching the experimental data, the energy partitioning observed by Trentelman, specifically the vibrational energy of the methyl fragments, was subsequently contradicted by the results of Hall *et al.*²⁰ Following the 193 nm photolysis of acetone-*d*₆ in a gas flow cell, the time dependent increase in the vibrationless state population was measured by absorption of the ν_2 fundamental. A significant increase, consistent with the time scale of vibrational relaxation, was observed and suggested that only 6% of CD₃ radicals were formed in the $v=0$ state. It was concluded that the nascent methyl radicals are “produced in a large number of vibrational states with no strong preference for any particular vibrational mode.”²⁰ The shortcomings of REMPI for extracting accurate vibrational state populations for the methyl radical, owing to the lack of information regarding the effects of predissociation and Franck–Condon factors, were cited as a possible source of the discrepancy in regard to the Trentelman data. Of course this observation necessitated a reassessment of the dissociation mechanism of acetone which was characterized by the authors as being fully stepwise, involving randomization sufficient to generate methyl radical fragments with near *prior* distributions in vibrational energy.

Despite the overlap of the two methyl radical translational energy distributions, their cumulative $P(E_T)$ still provides insight into the partitioning of the available energy in the dissociation process. The measured $\langle E_T \rangle$ of 7.7±0.5 kcal/mole for each methyl (Fig. 10) differs markedly from the $\langle E_T \rangle$ of 10.5±1.9 kcal/mole reported by Trentelman *et al.*¹⁹ The CH₃0₀ band origin, probed in that experiment, reflects the kinetic energy of *only the vibrationless methyl radicals*. If a large fraction of the available energy resides in the CH₃ fragments as Hall has suggested,²⁰ then the translational energy of the vibrationless methyl radicals is not rep-

representative of the overall dissociation dynamics. It is not surprising, therefore, that our measured $\langle E_T \rangle$ is substantially lower than the result of Trentelman. The average translational energy of the CO fragment, 4.8 ± 0.5 kcal/mole, is also considerably less than previously reported.¹⁹ Figure 12 shows a comparison between the derived $P(E_T)$ from this experiment and a Boltzmann distribution at 3000 K as suggested by the results of Trentelman. Although the peak of the two distributions are similar the 3000 K Boltzmann possesses a larger high energy contribution. Assuming that the combined average rotational and vibrational energy of the nascent CO fragments is ~ 9.0 kcal/mole,¹⁷⁻¹⁹ the total CH_3 internal energy content can be obtained using our derived average translational energies

$$\begin{aligned} \bar{E}_{\text{int}}(\text{CH}_3) &= \bar{E}_{\text{avail}} - \{2[\bar{E}_T(\text{CH}_3)] + \bar{E}_T(\text{CO}) + \bar{E}_{\text{int}}(\text{CO})\}, \\ E_{\text{int}}(\text{CH}_3) &= 52.8 - \{15.4 + 4.8 + 9.0\} = 23.6 \text{ kcal/mole}. \end{aligned} \quad (8)$$

As expected, our translational energies imply that the methyl fragments must contain appreciable internal excitation.

Stepwise versus concerted: If sufficient energy is deposited into a molecule to ensure the eventual cleavage of two bonds, the sequence of bond breaking is of fundamental mechanistic importance. It is particularly intriguing in the case of chemically equivalent bonds. A salient question in these systems is whether the bonds break in a *concerted* (synchronous or nonsynchronous) or a *stepwise* manner. Although Dewar⁴¹ has provided a commonly used description of each type of case, we adopt distinguishing definitions more suited to our technique.⁴² This involves rotation of the intermediate as gauge for the time delay, and hence the correlation between the first and second bond ruptures. Secondary bond cleavage that occurs before the intermediate, formed by the initial bond breaking, undergoes rotational averaging results in a strong correlation between the asymptotic velocity vectors of all three photofragments and is considered a *concerted* process.²²

An information theoretic approach to examine the correlation in molecular photodissociation predicted, using the experimental data, that acetone dissociation was intermediate between concerted and stepwise mechanisms.⁴² More recent calculations²⁰ have removed an overly severe approximation in the original calculations. The revised analysis was found to be consistent with a loss of angular correlation between the asymptotic velocity vectors of the CH_3 fragments, corresponding to complete rotational averaging in the second dissociation step. There is also experimental support for a stepwise dissociation at 193 nm. As discussed earlier, previous PTS studies of acetyl halides have demonstrated forward-backward symmetry in the secondary angular distribution at various average internal energies of the primary acetyl radical photoproduct. Acetyl chloride and acetyl bromide dissociated at 248 nm result in an average internal energy in the primary acetyl radical of 24 and 33 kcal/mole, respectively, and in both cases rotational averaging of the acetyl radical precedes secondary decomposition (Fig. 8). In light of the results of the previous section [specifically Eq. (8)] the primary dissociation of acetone at 193 nm will likely release an

average of ~ 8 kcal/mole in translation and ~ 12 kcal/mole to internal excitation of the primary methyl. As a consequence the acetyl radical fragment will contain $\langle E_{\text{int}} \rangle \sim 45$ kcal/mole. Thus, the most relevant acetyl halide comparison is the dissociation of acetyl iodide at 266 nm studied by Kroger and Riley where following primary dissociation the acetyl radicals have $\langle E_{\text{int}} \rangle \sim 44$ kcal/mole.^{29b} Kroger and Riley observed forward-backward symmetry in the secondary decomposition products demonstrating the lifetime of the acetyl radical to be comparable to or longer than the rotational period. The results of Kroger and Riley at a comparable internal energy of the acetyl radical intermediate to that of the 193 nm acetone dissociation suggest that the acetone data should be fit with a stepwise dissociation mechanism.

In order to fit the data at 193 nm with a stepwise mechanism it is first necessary to assume a primary $P(E_T)$ given the following considerations. Although the CH_3 fragments possess a high degree of internal excitation consistent with substantial redistribution of the available energy, the overall translational energy release is clearly greater than predicted by a statistical, prior, distribution. In fact the overall translational energy is not significantly different from the dissociation, involving the secondary decomposition of activated acetyl radicals, at 248 nm. If the energy disposal at 193 nm follows the trend seen at 266 and 248 nm, then one would expect statistical partitioning of the available energy superimposed onto the partitioning controlled by the two exit barriers on the potential energy surface. Since the initial bond cleavage in acetone at 193 nm, following internal conversion, eventually proceeds on the same potential energy surface as at 248 nm there is no reason *a priori* to expect a dramatic difference in the dissociation dynamics. The assertion of Trentelman that acetone containing ~ 50 kcal/mole of excess energy in the excited state should be insensitive to ~ 11 kcal/mole exit barrier is questionable since dissociation involves intersystem crossing, via out-of-plane motion, in conjunction with sufficient energy in the C-C stretching coordinate to surmount the barrier. We therefore assume a primary $P(E_T)$ at 193 nm based on the primary translational energy distributions measured for acetone at 266 and 248 nm suitably adjusted to the available energy. The resultant stepwise fits to the $m/e=15$ and $m/e=28$ TOF spectra are shown in Fig. 13. The primary $P(E_T)$ is peaked at 16 kcal/mole and is shown as the solid line in Fig. 14. The TOF data was then successfully fit with a forward/backward secondary distribution (shown in the insert in Fig. 14) and a secondary $P(E_T)$ peaked at 6 kcal/mole and shown as the dashed line in Fig. 14. The fit to the data was found to be sensitive to both the shape of the secondary $P(E_T)$ and the secondary angular distribution. The successful fitting of the data in this way, specifically the use of the near identical secondary $P(E_T)$ and the forward/backward $T(\theta)$ used to fit the data at 248 nm, provides strong evidence of a stepwise dissociation for acetone at 193 nm.

Model of the dissociation dynamics: In order to test further the validity of a stepwise mechanism and obtain information concerning the disposal of the internal energy we have applied a dynamical model to the dissociation of acetone at 193 nm. The nature of the dissociation requires a

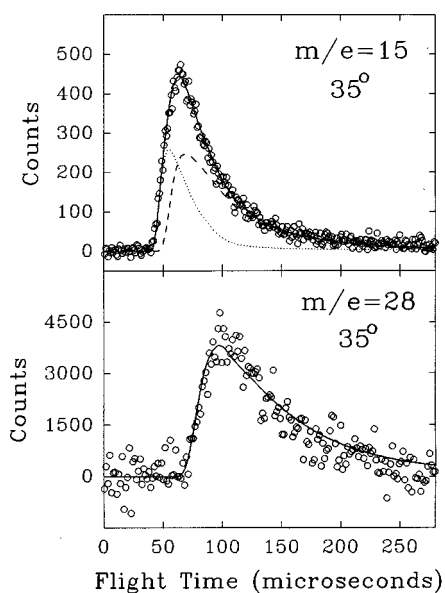


FIG. 13. TOF spectra at 193 nm of (a) $m/e=15$ (CH_3^+) and (b) $m/e=28$ (CO^+) at 35° . The open circles are the data. The contributions in (a) are CH_3 from reaction (1) (dotted line) and CH_3 from reaction (2) (dashed line). In (b) the solid line is CO from reaction (2). The $P(E_T)$'s and $T(\theta)$ used in the forward convolution fits are shown in Fig. 14.

model that reflects both the impulsive nature of reactions with large barriers to recombination as well as the statistical distribution of energy in excess of the barrier height. The present treatment represents a simple extension of the impulsive and statistical models that are currently employed.

The barrier impulsive model (BIM) is conceptually very simple. The total available energy is divided into two "energy reservoirs," one which is denoted *statistical* and the other *impulsive*

$$E_{\text{avail}}(\text{tot}) = E^{\text{stat}}(\text{tot}) + E^{\text{imp}}(\text{tot}). \quad (9)$$

The energy content of the first reservoir, $E^{\text{imp}}(\text{tot})$, is chosen to be the height of the exit barrier and it is assumed that once the molecule is beyond the transition state the lo-

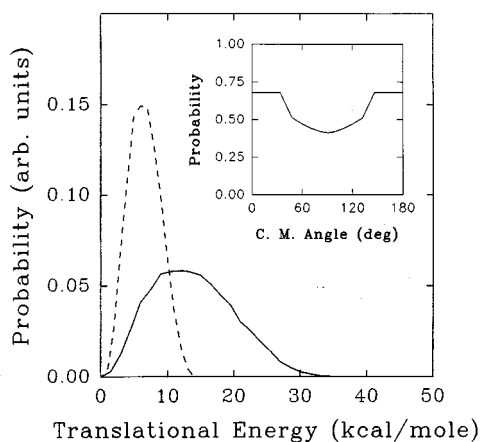


FIG. 14. Center-of-mass primary and secondary translational energy distributions derived from fitting the $m/e=15$ and $m/e=28$ TOF spectra shown in Fig. 13. The inset shows the secondary angular distribution.

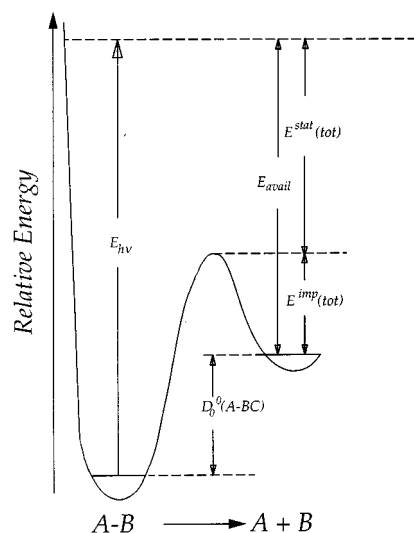


FIG. 15. Schematic diagram illustrating the relations between various energetic quantities in the barrier impulsive model.

calized release of the potential energy from the exit barrier can be adequately described by the impulsive model. The remaining energy, $E^{\text{stat}}(\text{tot})$, is then partitioned among the product R , V , and T degrees of freedom according to a simple statistical method. A schematic diagram illustrating the division of the available energy is shown in Fig. 15. By partitioning the energy in this way the model reduces to the impulsive model at the dissociation threshold and to a simplified statistical model in the absence of a barrier. Furthermore, since the translational energy of the products from the impulsive reservoir is fixed by the barrier height, the total translational energy increases with available energy statistically which is consistent with experimental observation. The impulsive reservoir can be partitioned among the fragment degrees of freedom according to either the soft or the rigid fragment models. The statistical reservoir is partitioned assuming that the energy is freely distributed among the *parent* modes up to the transition state. These vibrational modes are divided into three overlapping ensembles from which the statistical contributions to product R , V , and T are calculated. The average energies from each reservoir, which independently conserve linear and angular momentum, are combined to obtain the final average R , V , and T energies of the products. A more detailed description of the model is provided in the Appendix.

For the impulsive reservoir of the BIM, a barrier height of 13.2 kcal/mole was used based on the measurements of Zuckermann *et al.*⁵ A nonplanar dissociative geometry consistent with the geometry of the transition state was utilized in treating the impulsive reservoir.³ The impulse was assumed to be through the C_{3v} symmetry axis of the CH_3 group and therefore, resulted in no CH_3 rotational excitation. The statistical reservoir was partitioned using ground state acetone vibrational frequencies as an approximation to those of the $1,3(n, \pi^*)$ excited state.⁴³ Of the 24 modes of acetone, 6 disappear upon dissociation, evolving into product translation and rotation. Two of these modes, the symmetric and antisymmetric C-C stretch, were assigned to the translation

ensemble. Two methyl rocking modes, a methyl torsion, and the C–C–C skeletal bend were assigned to the rotational ensemble. The Beyer–Swinehart algorithm was used to calculate the vibrational density of states for all ensembles.³⁵ The moments of inertia for the CH₃CO fragment were determined from the *ab initio* equilibrium geometry calculated by Baird and Kathpal.⁴⁴ Vibrational frequencies of the parent were those used in the RRKM calculations of Watkins and Word.⁹ The secondary bond cleavage assumed a total available energy equal to the average internal energy of the acetyl fragment from the initial step minus the endothermicity of the reaction. An exit barrier height of 6 kcal/mole, derived from Ref. 13, was used for acetyl dissociation.

The results of the model and, for comparison, the average translational energies of the photofragments derived from the stepwise fitting procedure are shown in Table I. The predictions from the model are in good agreement with the experimental results. This is not too surprising since the translational energy release in each step closely matches the corresponding exit barrier height. More interesting are the calculated average internal energies which show that, assuming the complete randomization of available energy in excess of the barriers, the initial methyl possesses substantially more internal excitation than the second. The total internal energy in the methyl fragments according to the model is 26.6 kcal/mole, which is consistent with the results of Hall *et al.* but much higher than the 6.2 kcal/mole predicted by the Trentelman model.

V. CONCLUDING REMARKS

At 248 nm ($S_1 \leftarrow S_0$) acetone dissociates to produce a methyl and acetyl radical. On average 14.2 ± 1.0 kcal/mole is observed in photofragment translation. The similarity of this value to the height of the exit barrier and its invariance when compared to excitation at longer wavelengths in the same absorption band strongly suggests that the energy partitioning, specifically the translational energy release, is mediated by the exit barrier on the potential energy surface. Of the nascent acetyl radicals $30\% \pm 4\%$ have sufficient internal energy to undergo secondary decomposition. An upper limit to the CH₃CO barrier to dissociation has been determined to be 17.8 ± 3.0 kcal/mole, in agreement with the 17 ± 1 kcal/mole value derived from the photodissociation of acetyl chloride. The translational energy of the CH₃ and CO fragments arising from the decomposition of the nascent acetyl radicals is consistent with the magnitude of the exit barrier.

Following excitation at 193 nm acetone was observed to dissociate exclusively into two methyl radicals and carbon monoxide. The average translational energies for the photofragments were found to be considerably less than determined previously, suggesting that a significant fraction of the available energy is partitioned into methyl internal excitation in agreement with the work of Hall *et al.* A stepwise method of analysis, using only slightly modified energy and angular distributions analogous to those derived at 248 nm, was successful in fitting the experimental data. We, therefore, conclude that the mechanism of dissociation at 193 nm can be characterized as fully stepwise, involving substantial randomization of the available energy and complete rotational

averaging in the second step. Consequently, the dissociation dynamics of acetone at 193 nm can be viewed as a simple extension of the mechanisms that occur at both 266 and 248 nm giving credence to the notion that even modest exit barriers can greatly influence the partitioning of the available energy in photodissociation processes.

ACKNOWLEDGMENTS

The authors gratefully acknowledge Dr. G. E. Hall and Dr. A. G. Suits for many fruitful discussions. J.D.G. and S.W.N. acknowledge H. Reisler, R. Harris, and W. H. Miller for helpful discussions. This work was supported by the Director, Office of Energy Research, Office of Basic Energy Sciences, Chemical Sciences Division of the U.S. Department of Energy under Contract No. DE-ACO3-76SF00098.

APPENDIX

The statistical reservoir. The partitioning of the statistical reservoir between the two fragments relies upon ideas developed for the separate statistical ensembles method (SSE),⁴⁵ phase space theory (PST),⁴⁶ and the prior distribution.⁴⁷ The prior distribution and PST, which assume a loose transition state, include only information regarding the product states, without treating explicitly the vibrational modes of the parent molecule that develop asymptotically into product rotation and translation. The SSE method assumes that vibrations become adiabatic prior to rotations and uses different ensembles to calculate the vibrational and rotational distributions. The basic assumption of our method of partitioning the statistical reservoir is that the energy is distributed statistically in the *parent* molecule up to the transition state. The breaking of the bond is viewed as an instantaneous event, which prevents any further rearrangement of energy. Following this reasoning, it makes sense to partition the statistical energy into T , R , and V at the transition state using information only from the parent, and not information from the products as in PST and the prior distribution. The method used to divide the statistical reservoir into T , R , and V is very similar to the SSE procedure. Product vibrations can develop out of all parent vibrational modes, while product rotations and translations develop only out of those modes of the parent molecule that disappear during the course of the reaction.

Three ensembles are utilized. The vibrational ensemble includes all vibrational modes of the parent and overlaps with the other two ensembles. The rotational ensemble includes those disappearing modes that lead to rotational excitation of the products. These modes can include methyl torsions, skeletal bends, etc. The third ensemble is a translational ensemble that includes modes that disappear into product translations. Identification of which modes belong in which ensemble can be a subtle matter for large parent molecules, but three basic rules can be easily applied:

- (1) parent torsions and skeletal bends go into the “rotational” ensemble,
- (2) parent skeletal stretches go into the “translational” ensemble, and

(3) *all* parent vibrational modes go into the “vibrational” ensemble.

Here we have made the rather severe assumption that beyond the transition state bends and torsions evolve *adiabatically* into product rotations. For torsions this approximation is not unreasonable but for skeletal bends the impulsive nature of the potential energy surface should effectively

couple rotation and translation. Consequently, this results in an overestimation of photofragment rotation at the expense of translational energy. Although attempts can be made to correct this deficiency, we do not anticipate that this will significantly alter the average energy quantities.

The statistical energy reservoir is partitioned into rotations in the following manner:

$$\langle E_R^{\text{stat}} \rangle = \frac{\int_0^{E^{\text{stat}}} dE_V \int_0^{E^{\text{stat}}-E_V} dE_T \int_0^{E^{\text{stat}}-E_V-E_T} dE_R \rho_P(E_V) \rho_R(E_R) \rho_T(E_T) \delta(E^{\text{stat}}-E_V-E_T-E_R) E_R}{\int_0^{E^{\text{stat}}} dE_V \int_0^{E^{\text{stat}}-E_V} dE_T \int_0^{E^{\text{stat}}-E_V-E_T} dE_R \rho_P(E_V) \rho_R(E_R) \rho_T(E_T) \delta(E^{\text{stat}}-E_V-E_T-E_R)}, \quad (\text{A1})$$

where ρ_P , ρ_R , and ρ_T are the densities of states for the *P* (parent), *R*, and *T* ensembles of parent vibrational modes. The *P* ensemble is made up of all vibrational modes of the parent molecule. In the harmonic approximation, the densities of states can be computed easily using the Beyer–Swinehart algorithm. The expressions for $\langle E_V^{\text{stat}} \rangle$ and $\langle E_T^{\text{stat}} \rangle$ are similar to the one for the rotational energy that is given above.

Essentially, it is assumed that the energy above the barrier is going to be distributed statistically between the three ensembles, where the ensemble for vibrations can sample from the other two ensembles. The statistics, and hence the energy distribution, are governed by the vibrational frequencies of the parent as well as a judicious choice of modes for membership in each ensemble.

Dividing $\langle E_T^{\text{stat}} \rangle$ between the two fragments is easily accomplished by conserving linear momentum and $\langle E_R^{\text{stat}} \rangle$ is similarly partitioned by requiring conservation of angular momentum.

The only remaining difficulty is to divide the vibrational energy from the statistical reservoir between the two fragments. It seems reasonable to view the impulse as an instantaneous event, so that the energy is frozen in the parent modes. The energy in the modes that develop into fragment vibrations should then be assigned to the appropriate fragment. Identifying these modes and obtaining their frequencies seems to be impossible for all but the simplest of molecules. By approximating the frequencies of these modes at the transition state by the frequencies of the fragment modes themselves, one obtains the following expression for the vibrational energy partitioned into fragment *A* from the statistical reservoir:

$$\langle E_V^{\text{stat}}(A) \rangle = \frac{\int_0^{E^{\text{stat}}} dE_A \int_0^{E^{\text{stat}}-E_A} dE_B \rho_A(E_A) \rho_B(E_B) \delta(E^{\text{stat}}-E_A-E_B) E_A}{\int_0^{E^{\text{stat}}} dE_A \int_0^{E^{\text{stat}}-E_A} dE_B \rho_A(E_A) \rho_B(E_B) \delta(E^{\text{stat}}-E_A-E_B)}, \quad (\text{A2})$$

where ρ_A and ρ_B are the vibrational densities of states of fragments *A* and *B*, respectively.

The impulsive reservoir. The basic premise of the standard impulsive model is that all of the available energy is released as a repulsion localized in the reaction coordinate.^{37,38} For the present model, the available energy is replaced with the height of the exit barrier. In the rigid fragment limits the dissociation results in no vibrational excitation of the fragments. The impulsive reservoir is therefore partitioned only between fragment rotation and translation

$$E^{\text{imp}}(\text{tot}) = E_T^{\text{imp}}(\text{tot}) + E_R^{\text{imp}}(A) + E_R^{\text{imp}}(B), \quad (\text{A3})$$

$$E^{\text{imp}}(\text{tot}) = \frac{1}{2} \mu_{AB} g^2 + \frac{(J_A)^2}{2I_A} + \frac{(J_B)^2}{2I_B}, \quad (\text{A4})$$

where g is the relative velocity of *A* and *B*. Since the dissociation must conserve angular momentum (initially assumed to be zero) the translational energy is constrained as follows:

$$E_T^{\text{imp}}(\text{tot}) = \frac{E^{\text{imp}}(\text{tot})}{1 + [(b_A)^2 \mu_{AB}/I_A] + [(b_B)^2 \mu_{AB}/I_B]}, \quad (\text{A5})$$

where b_A and b_B are the exit impact parameters. Hence, the translational energy of the products predicted by the rigid

fragment model is intimately dependent on the choice of the dissociative geometry. Once the translational energy has been determined, the rotational energy of the fragments can be expressed in terms of $E_T^{\text{imp}}(\text{tot})$

$$E_R^{\text{imp}}(A) = E_T^{\text{imp}}(\text{tot}) \frac{(b_A)^2 \mu_{AB}}{I_A}, \quad (\text{A6})$$

$$E_R^{\text{imp}}(B) = E_T^{\text{imp}}(\text{tot}) \frac{(b_B)^2 \mu_{AB}}{I_B}. \quad (\text{A7})$$

The two reservoirs are then combined to give average translational energies for the two fragments as follows:

$$E_T(A) = E_T^{\text{stat}}(A) + E_T^{\text{imp}}(A), \quad (\text{A8})$$

$$E_T(B) = E_T^{\text{stat}}(B) + E_T^{\text{imp}}(B). \quad (\text{A9})$$

Similar equations are used for rotational and vibrational energies.

Test case: Acetic acid. The present model was also used to compare predicted energy partitioning with experimental results in the photodissociation of acetic acid at 218 and 200 nm.^{48,49} Both wavelengths involve $^1(n, \pi^*)$ excitation but differ by ~ 12 kcal/mole in the energy available for dissocia-

TABLE II. Product energy partitioning for acetic acid photodissociation at 200 and 218 nm.

	E_R (OH)	E_V (OH)	E_T (OH)	E_{int} (CH ₃ CO)	E_T (CH ₃ CO)
Experiment ^a					
218 nm	1.21 ^b	<0.2	9.81	12.9	3.89
200 nm	1.36	<0.4	10.4	23.73 ^c	4.11
BIM					
218 nm	1.39	0.23	9.79	12.73	3.87
200 nm	2.05	0.80	10.15	22.99	4.01
SFIM					
218 nm	0.08	0.63	11.30	11.53	4.46
200 nm	0.12	0.90	16.14	16.47	6.38

^aReferences 48 and 49.^bAll energies are expressed in kcal/mole.^cInferred from E_{avail} and all other measured quantities.

tion. The barrier height was assumed to be 13.0 kcal/mole and the dissociative geometry was nonplanar. Vibrational frequencies were taken from Herman and Hofstadter⁵⁰ with the mode assignments of Haurie and Novak.⁵¹ The C–O(H) stretch and the COO bend were assumed to evolve into product translation while the OH torsion and rocks were partitioned into rotation. The OH and CH₃CO vibrational density of states were calculated using the method of Beyer–Swinehart. Table II shows the BIM results and includes predictions of the soft fragment impulsive model (SFIM). The favorable agreement of the model to the experimental results of Hunnicutt *et al.* suggest that the barrier impulsive model has general applicability for those cases that involve impulsive-type potential energy surfaces. We expect that this model will work for systems like the two shown above that satisfy several criteria: (1) IVR should occur prior to dissociation, (2) the molecules should be large enough to contain many modes that are not directly involved in the dissociation, and (3) the dynamics beyond the transition state should permit facile treatment of the impulsive reservoir. The photodissociation of carbonyl compounds, excited to their $^1(n, \pi^*)$ state, appears to be well suited for the above treatment. In general these molecules dissociate over a barrier that results from an avoided crossing between the $^3(n, \pi^*)$ and $^3(\sigma, \sigma^*)$ configurations in nonplanar geometries. Since the dissociation ultimately involves the cleavage of only a single bond, the impulsive model can be used in a straightforward manner. In addition, the lack of measured anisotropy in the photodissociation of these compounds suggests that the excited state should exist for sufficient time to allow almost full randomization of the initial excitation energy.

¹J. G. Calvert and J. N. Pitts, *Photochemistry* (Wiley, New York, 1966).²E. K. C. Lee and R. S. Lewis, *Adv. Photochem.* **12**, 1 (1980).³M. Reinsch and M. Klessinger, *J. Phys. Org. Chem.* **3**, 81 (1990).⁴J. Michl and V. Bonacic-Koutecky, *Electronic Aspects of Organic Photochemistry* (Wiley, New York, 1990), p. 378.⁵H. Zuckermann, B. Schmitz, and Y. Hass, *J. Phys. Chem.* **92**, 4835 (1988).⁶G. Hancock and K. R. Wilson, in *Proceedings, IVth International Symposium on Molecular Beams Cannes, France, 1973*.⁷L. D. Waits, R. J. Horwitz, and J. A. Guest, *Chem. Phys.* **155**, 149 (1991).⁸J. Solomon, C. Jonah, P. Chandra, and R. Bersohn, *J. Phys. Chem.* **55**, 1908 (1971).⁹K. W. Watkins and W. M. Word, *Int. J. Chem. Kinet.* **6**, 855 (1974).¹⁰P. Cadman, C. Dodwell, A. F. Trotman-Dickenson, and A. J. White, *J. Chem. Soc. A* **14**, 2371 (1970); H. E. O'Neal and S. W. Benson, *J. Chem. Phys.* **36**, 2196 (1962); J. G. Calvert and J. T. Gruver, *J. Am. Chem. Soc.* **80**, 1313 (1958); J. A. Kerr and J. G. Calvert, *J. Phys. Chem.* **69**, 1922 (1965); H. M. Frey and I. C. Vinnal, *Int. J. Chem. Kinet.* **5**, 523 (1973); L. Szivovics and R. Walsh, *Faraday Trans. I*, **70**, 33 (1974).¹¹A. Gandini and P. A. Hackett, *J. Am. Chem. Soc.* **99**, 6185 (1977).¹²S. Deshmukh and W. P. Hess, *J. Chem. Phys.* **100**, 1 (1994).¹³S. W. North, D. A. Blank, and Y. T. Lee, *Chem. Phys. Lett.* **222**, 38 (1994).¹⁴G. A. Gaines, D. J. Donaldson, S. J. Strickler, and V. Vaida, *J. Chem. Phys.* **92**, 2762 (1988).¹⁵D. J. Donaldson, G. A. Gaines, and V. Vaida, *J. Chem. Phys.* **92**, 27266 (1988).¹⁶P. D. Lightfoot, S. P. Kirwan, and M. J. Pilling, *J. Phys. Chem.* **92**, 4938 (1988).¹⁷D. J. Donaldson and S. R. Leone, *J. Phys. Chem.* **85**, 817 (1986).¹⁸E. L. Woodbridge, T. R. Fletcher, and S. R. Leone, *J. Chem. Phys.* **92**, 5387 (1988).¹⁹K. A. Trentelman, S. H. Kable, D. B. Moss, and P. L. Houston, *J. Chem. Phys.* **91**, 7498 (1989).²⁰G. E. Hall, D. Vanden Bout, and T. J. Sears, *J. Chem. Phys.* **94**, 4182 (1991).²¹Y. T. Lee, J. D. McDonald, P. R. LeBreton, and D. R. Herschbach, *Rev. Sci. Instrum.* **40**, 1402 (1969).²²S. W. North, C. A. Longfellow, and Y. T. Lee, *J. Chem. Phys.* **99**, 4423 (1993).²³D. Proch and T. Trickl, *Rev. Sci. Instrum.* **60**, 713 (1989).²⁴A. M. Wodtke, Ph.D. thesis, University of California, Berkeley, 1986; X. Zhao, Ph.D. thesis, University of California, Berkeley, 1988.²⁵X. Zhao, G. M. Nathanson, and Y. T. Lee, *Acta Physicochim. Sinica* **8**, 70 (1992).²⁶S. W. Benson and A. Amano, *J. Chem. Phys.* **36**, 3464 (1962); *JANAF Thermochemical Tables*, 2nd ed., Natl. Stand. Ref. Data Sr. U.S. Natl. Bur. Stand. 37 (U.S. GPO, Washington, D.C., 1971).²⁷J. D. Swaley and C. C. Costain, *J. Chem. Phys.* **31**, 1562 (1959); F. F. Cleveland, M. J. Muray, J. R. Coley, and V. I. Komarewsky, *ibid.* **10**, 18 (1942); P. Cossee and Schechtschneider, *ibid.* **44**, 97 (1966).²⁸R. N. Zare, Ph.D., Harvard University, 1964; R. N. Zare, *Mol. Photochem.* **4**, 1 (1972).²⁹(a) W. B. Miller, S. A. Safron, and D. R. Herschbach, *Chem. Soc., Faraday Disc.* **44**, 108 292 (1967); *J. Chem. Phys.* **56**, 3581 (1972); (b) P. M. Kroger and S. J. Riley, *ibid.* **67**, 4483 (1977); (c) *ibid.* **70**, 3863 (1979); (d) E. J. Hints, X. Zhao, and Y. T. Lee, *ibid.* **92**, 2280 (1990).³⁰S. W. North, D. A. Blank, and Y. T. Lee (unpublished results).³¹D. A. Blank, S. W. North, and Y. T. Lee, *Chem. Phys.* **122**, 35 (1994); S. W. North, D. A. Blank, and Y. T. Lee, *J. Chem. Phys.* **102**, 791 (1995); R. E. Continetti, B. A. Balko, and Y. T. Lee, *Chem. Phys. Lett.* **182**, 400 (1991).³²At sufficiently high laser fluences a two photon signal corresponding to the photodissociation of the methyl radical was observed.³³X. Zhao, W. B. Miller, E. J. Hints, and Y. T. Lee, *J. Chem. Phys.* **90**, 5527 (1989).³⁴By constraining acetone to be symmetric (C_{2v}) the equivalence of the two methyls is ensured.³⁵P. J. Robinson and K. A. Holbrook, *Unimolecular Reactions* (Wiley-Interscience, London, 1972); R. D. Gilbert and S. C. Smith, *Theory of Unimolecular and Recombination Reactions* (Blackwell, Boston, 1990).³⁶G. M. Breuer and E. K. C. Lee, *J. Chem. Phys.* **75**, 989 (1971).³⁷G. E. Busch and K. R. Wilson, *J. Phys. Chem.* **56**, 3626 (1972).³⁸A. F. Tuck, *J. Chem. Soc., Faraday Trans.* **73**, 689 (1977).³⁹T. K. Minton, P. R. Felder, R. J. Brudzynski, and Y. T. Lee, *J. Chem. Phys.* **81**, 1759 (1984).⁴⁰M. Baba, H. Shinohara, N. Nishi, and N. Hirota, *Chem. Phys.* **83**, 221 (1984).⁴¹M. J. S. Dewar, *J. Am. Chem. Soc.* **106**, 209 (1984).⁴²C. E. M. Strauss and P. L. Houston, *J. Phys. Chem.* **94**, 8751 (1990).⁴³P. Cossee and J. H. Schachtschneider, *J. Chem. Phys.* **44**, 97 (1966).⁴⁴N. C. Baird and H. B. Kathpal, *Can. J. Chem.* **55**, 863 (1977).⁴⁵C. Wittig, I. Nadler, H. Reisler, M. Noble, J. Catanzarite, and G. Radhakrishnan, *J. Chem. Phys.* **83**, 5581 (1985).⁴⁶P. Pechukas and J. C. Light, *J. Chem. Phys.* **42**, 2608 (1965); P. Pechukas, C. Rankin, and J. C. Light, *ibid.* **44**, 794 (1966).

⁴⁷R. D. Levine and J. L. Kinsey, in *Atomic–Molecular Collision Theory—A Guide for the Experimentalist* (Plenum, New York, 1979).

⁴⁸S. S. Hunnicutt, L. D. Waits, and J. A. Guest, *J. Phys. Chem.* **93**, 5188 (1989).

⁴⁹S. S. Hunnicutt, L. D. Waits, and J. A. Guest, *J. Phys. Chem.* **95**, 562 (1991).

⁵⁰R. C. Herman and R. Hofstadter, *J. Chem. Phys.* **7**, 460 (1939).

⁵¹M. Haurie and A. Novak, *Spectrochim. Acta* **21**, 1217 (1965).